
ELSEVIER

Nuclear Instruments and Methods in Physics Research B 184 (2001) 421–429

NIM B
Beam Interactions with Materials & Atoms

www.elsevier.com/locate/nimb

Combined photothermal and photoacoustic characterization of silicon–epoxy composites and the existence of a particle thermal percolation threshold

M.E. Rodríguez [a,*], P.J. Mendoza [a], A. Mandelis [b], L. Nicolaides [b]

[a] *Departamento de Fisica Aplicada y Tecnologia Avanzada, Universidad National Autonoma de México, Apdo Postal 0-1010, Querétaro, Querétaro 76001, Mexico*

[b] *Photothermal and Optoelectronic Diagnostic Laboratories, Department of Mechanical and Industrial Engineering, University of Toronto, Ont., Canada M5S 3G8*

Received 9 February 2001; received in revised form 21 May 2001

Abstract

Photoacoustic (PA) and photothermal radiometric (PTR) detection were used to characterize thermal properties of silicon–epoxy composite materials in the volume range $0\% < x < 32$ vol% (50 μm). PA detection was used to study the variation of the thermal diffusivity as a function of Si volume fraction, and PTR was used to determine the influence of the electronic carrier contribution to the thermal transport with the optical properties taken into consideration. The combined PA and PTR measurements show that there exists no linear relation between thermal diffusivity and silicon volume fraction. Thermal diffusivity and optical absorption coefficient measurements can be obtained by means of combined PA and PTR measurements. Both parameters exhibit anomalous behavior in the 16% Si volume fraction range, corroborating the existence of a particle percolation threshold for three-dimensional random close packed (rcp) solids.

PACS: 12.60.R; 81.20; 64.60.A
Keywords: Thermal diffusivity; Composite; Percolation

1. Introduction

Photothermal radiometry (PTR) and other photoacoustic (PA) techniques are widely used in the investigation of material properties. Their non-contact and non-invasive character makes these techniques very useful for measuring thermal and carrier diffusion coefficients, minority carrier lifetime, front surface recombination velocity and thermal diffusivity. Therefore, PTR and PA techniques have been used extensively to determine the foregoing parameters in semiconductor silicon [1,2]. The PA technique has also been used to study thermal properties in composite materials

* Corresponding author. Tel.: +52-4-224-1645; fax: +52-4-212-1111.
E-mail address: mariorod@cicataqro.ipn.mx (M.E. Rodríguez).

0168-583X/01/$ - see front matter
PII: S0168-583X(01)00726-1

such as CdTe–Te [4]. The importance of composite materials for electronic applications has grown in recent years. Composite materials are used in the electronics industry for resistors, sensors, transducers and substrates [3–5]. Composite materials have been developed in many forms with a variety of particle sizes, volume fractions, shapes and topologies that depend on the particular processing route used to fabricate the materials. Understanding the effects of each of these parameters on the thermal and electrical transport properties of these materials is an important problem, both for fundamental reasons and for the implications in industrial applications.

In this work, we study the thermal diffusivity and electrical resistivity of silicon–epoxy composite materials as a function of the silicon volume fraction. We also perform a qualitative analysis of the PTR signal amplitude and phase. At low carrier densities, the thermal conductivity of crystalline silicon (isotropic) can readily be described in terms of phonon conductivity where the phonon mean-free-path is limited mainly by scattering with other phonons, various impurities and imperfections, and by the crystal boundaries [6]. Similarly, thermal conduction in epoxy involves the lattice. In composite materials the electrical and thermal transport properties have a spatial dependence, and thus it is necessary to refer to these properties as "effective". In the case of composite materials forming electrically insulating phases, the Wiedemann–Franz law cannot be used to determine the electronic contribution to thermal transport (conductivity), k_e, as it is only applicable to continuous and electrically conducting materials. Phenomenological percolation theory has been used to explain the electrical behavior of composites as a function of the included phase in a material formed by two phases (insulator–conductor) [4]. It is clear that in the case of electric carriers the existence of a continuous path is necessary in order to have current continuity. At the percolation threshold value, the existence of this path allows carrier movement through the bulk, resulting in a strong change in the electrical resistivity. However, in the case of thermal transport in composite materials, it is necessary to take into account the character of each type of carrier (electrons, holes, phonons) associated with thermal transport. It is known that the interfacial thermal contact resistance (ITCR) between different constituent phases in a composite can arise from the combination of poor mechanical or chemical adhesion at the interface, as well as from thermal expansion mismatch [5]. The existence of such thermal barriers leads to a lowering of the effective thermal diffusivity (conductivity) of the composite.

2. Sample preparation

The silicon–epoxy system is formed using epoxy base resin and silica low-vapor-pressure resin (Torr-seal, Varian Vacuum systems) used in vacuum applications, with high electrical resistivity (10^{12} Ω cm), and crystalline p-silicon (22–40 Ω cm). This kind of epoxy is preferred owing to its very low porosity, so that the final composite can be considered biphasic (without air). Fig. 1 shows an optical micrograph of an epoxy–silicon composite system consisting of 32 vol% silicon (250 μm × 250 μm). The bright regions correspond to silicon particles and the dark regions correspond to the epoxy material. Samples were prepared using a mixture of silicon powders obtained from a p-Si wafer (micrometer-size particles, see Table 1) and Torr-seal epoxy. The dimensions of silicon particles were selected with sizes between 50 and 75 μm, using meshes, which were verified by using a particle size distribution CILAS 1064 system with pure water and dry measurements. According to the image (see Fig. 1), these particles do not have a regular shape. Silicon powder was randomly mixed with the semi-liquid epoxy, and the mixture was molded using acetate films, 2 cm in diameter and 600 μm thick. The samples were left to cure at room temperature.

3. Experimental setup

Fig. 2 shows the experimental setup used for PA and photothermal measurements. A harmonically modulated argon ion laser beam was obtained using an acousto-optic modulator (AOM). For PTR detection, a 10× beam expander was used to obtain a

Fig. 1. Optical micrograph of a silicon–epoxy composite (250 μm × 250 μm). Bright spots correspond to silicon particles and dark areas correspond to the epoxy matrix.

Table 1
Values of physical parameters for crystalline Si, SiO_2, epoxy and composite materials

Sample	Volume fraction (%)	Thickness (μm)	α (cm^2/s)	β (cm^{-1}) $\lambda = 514.5$ nm
Silicon		309 ± 5	0.923	10^4 [1]
SiO_2			0.004 [6]	
Epoxy		410 ± 4	0.0021	
Epoxy (white)			0.0024 [1]	
Epoxy (black)			0.0021 [1]	
Silicon–epoxy-1	6.100	408 ± 5	0.0163 ± 0.00093	
Silicon–epoxy-2	9.350	430 ± 5	0.0178 ± 0.00103	70
Silicon–epoxy-3	12.74	357 ± 6	0.0169 ± 0.00110	200
Silicon–epoxy-4	15.71	537 ± 5	0.0340 ± 0.00245	130
Silicon–epoxy-5	19.12	433 ± 4	0.0275 ± 0.00131	200
Silicon–epoxy-6	22.41	477 ± 6	0.0290 ± 0.00197	260
Silicon–epoxy-7	32.15	502 ± 4	0.0523 ± 0.00336	700

1 cm beam diameter incident on the sample. The spot size of the exciting laser beam used for PA measurements was approximately 3 mm (Gaussian beam). As a result, the beam size was much larger than the particle size in the composite and satisfied the theoretical condition for the one-dimensional PTR model. The open photoacoustic cell (OPC) and PTR infrared detector output voltages were measured using a lock-in amplifier (SR 850). The frequency-scan bandwidth was 6 Hz to 1.5 kHz for PA, and 10 Hz to 100 kHz for PTR measurements. The data acquisition procedure was automated. The main difference between this setup and conventional PA systems [7–11] was the use of the AOM for extended frequency scans, and the gradium lens to control beam size, in order to assure one-dimensional conditions for theoretical modeling [10,11]. All resistivity measurements were carried out using a four-point-probe method and ohmic contacts were made using silver paint.

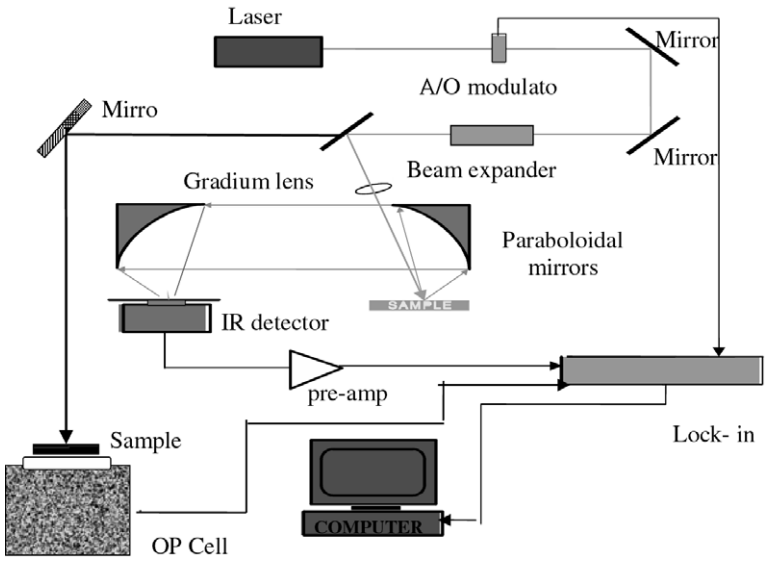

Fig. 2. Experimental setup for the radiometric and PA measurements.

4. Theoretical model

For the case of optically opaque and thermally thick solids, it has been shown [12] that PA detection can yield the thermal diffusivity, α, of a sample through a frequency scan and fitting of the photoacoustic signal (PAS), data to a simple expression:

$$\mathrm{PAS} = \frac{A}{f}\mathrm{e}^{-G\sqrt{f}}, \tag{1}$$

where $G = \sqrt{\pi l^2/\alpha}$, l is the thickness of the sample, f is the modulation frequency and A includes all other factors, such as gas thermal properties, laser power and instrumental factors.

The physical foundations of signal generation in laser PTR of semiconductors have been described elsewhere [2,13]. Briefly, when an absorbing solid is irradiated by modulated light, it simultaneously produces heating (thermal-wave component) due to direct lattice absorption and non-radiative conversion, as well as a modulation in the free photoexcited carrier density (plasma-wave component), provided the photon energy is greater than the bandgap energy. The modulated temperature rise can be monitored through the infrared (IR) blackbody (Planck) emission from the material, by measuring variations in the IR radiant emittance. The photoexcited plasma density-wave further produces infrared photons through de-excitation to defect or impurity states, which are collected and registered as a change in the modulated IR emissivity of the electronic solid. Thus, it is possible to obtain information about the thermal and electronic transport properties by means of PTR detection. The thermal contribution for this type of samples is strongest at the low-frequency end of the spectrum of the experimental data. The PTR signal is further influenced by the optical properties of the sample, and thus it is important to study how these properties vary as the volume percentage changes. A theoretical model [14] that takes into consideration the optical and thermal properties of the sample is used to fit the low-frequency end of the PTR data.

5. Experimental results and discussion

5.1. Electrical characterization

The electrical resistivity values for our composites across the studied range was found to be $>10^8$ Ω cm. The resistivity of silicon used in the

experiments was 22–40 Ω cm, while that of the epoxy was 10^{12} Ωcm. The resistivity values for the epoxy–silicon composite materials found in our experiments were not expected on the basis of the above-mentioned measured values for silicon and epoxy. We were expecting an electrical three-dimensional percolation transition (insulator–semiconductor) for a random close packed system (rcp) [3,18]. This electrical transition, however, did not appear due to the fact that the silicon particles used in these composites had a native thin oxide film on their surface, which grew during the sample fabrication process. This thin oxide film has a resistivity between 10^{15}–10^{17} Ω cm, a very low thermal conductivity of 0.014 W/cm K [15], and a thermal diffusivity of 0.004 cm^2/s at room temperature [16,17]. The thin oxide layer acts as an electrical barrier for carriers, preventing the possible insulator–semiconductor transition [3,18].

5.2. PA characterization

The amplitude of the PA modulation frequency scan for a p-Si wafer used in these experiments (sample thickness was 309 μm) is plotted in Fig. 3. According to Fig. 3, the PA signal amplitude exhibits two slightly different modulation frequency regimes. For frequencies lower than approximately 234 Hz, the frequency response obeys the $f^{-1.5}$ behavior, typical of the thermally thin regime [12], where the sample thickness (l) is much smaller than the thermal diffusion length ($\mu = \sqrt{\alpha/\pi f}$): $l \ll \mu$. Between 240 and 700 Hz, an essentially exponential behavior, characteristic of the thermally thick regime according to Eq. (1), is seen (transmission measurements). The best fit of the experimental data yielded a value of $\alpha = 0.923$ cm^2/s for the thermal diffusivity of the Si sample.

Fig. 4 shows the PA modulation frequency dependence of an optically opaque silicon–epoxy composite material containing 32 vol% silicon (502 μm thickness). It is seen that in this case three different frequency regimes appear. In region I, for frequencies lower than 10 Hz, the sample is thermally thin (cut-off frequency 6.8 Hz). In region II, the sample exhibits thermally thick behavior. Finally, in region III the main contribution arises from thermal surface sources due to the existence

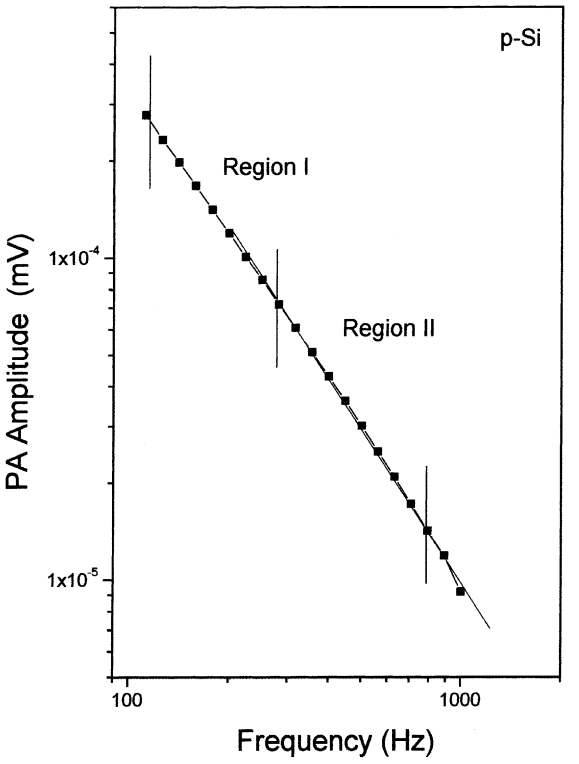

Fig. 3. The PA signal amplitude for crystalline silicon as a function of modulation frequency.

of Si particles close to the surface. For this sample, the thermal diffusivity obtained from the experimental data fit to Eq. (1) was $\alpha = 0.0523$ cm^2/s.

The same procedure using Eq. (1) was applied to a number of other samples. The experimental values of the thermal diffusivity obtained for each sample corresponds to an average of three measurements (see Table 1). For samples with low silicon volume fraction ($x < 10$ vol%) it was necessary to add a thin aluminum foil on the surface using a thermal paste, due to the optical semitransparency of these samples. In Fig. 5 we summarize the photoacoustically measured thermal diffusivity of the epoxy–silicon composites as a function of silicon volume fraction. The thermal analysis of these composites resulted in three regions: region I with $x < 10\%$ volume fraction (Maxwell dilute limit) [3], followed by region II with 10 vol% $< x <$ 20 vol%, which is followed by region III for $x > 20$ vol%. This division originates

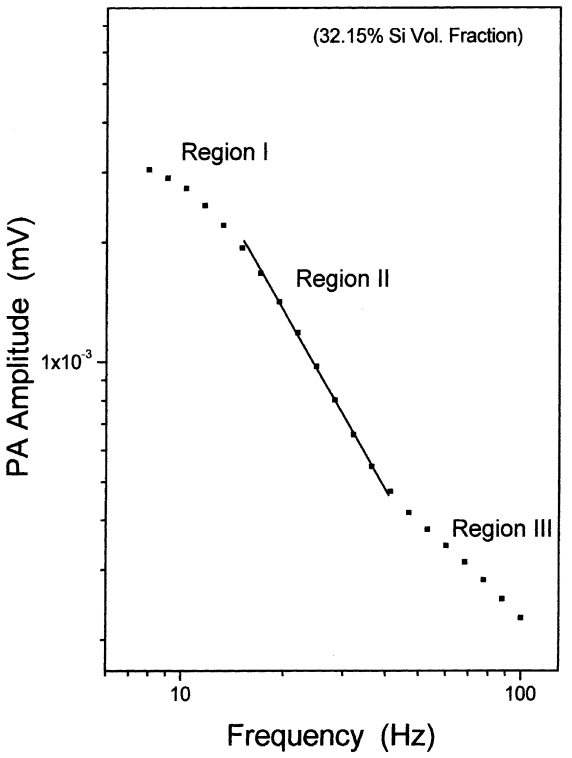

Fig. 4. The PA signal amplitude frequency response for a silicon–epoxy composite material, in which the silicon volume fraction is 32 vol%. The various regions are discussed in the text.

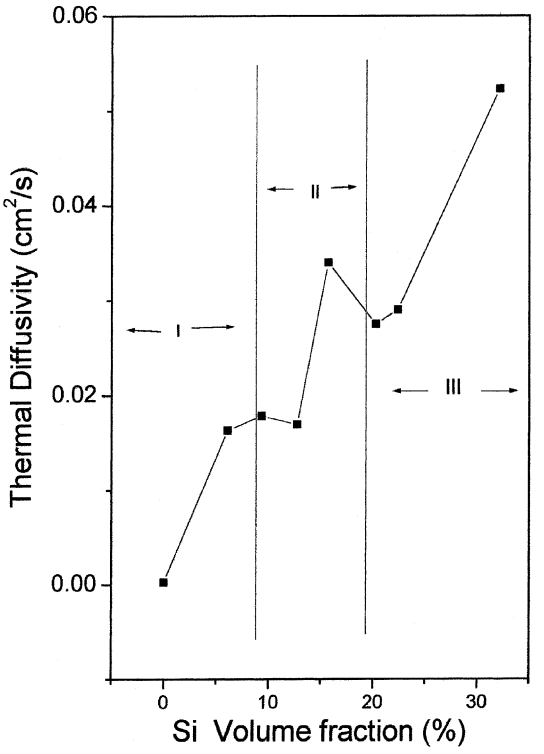

Fig. 5. Thermal diffusivity values of various silicon–epoxy composite materials as extracted from best fits of data such as those in region I, Fig. 4, using Eq. (1).

in the average number of contacts per particle (M) [3,4]). For $x < 10$ vol% it is expected that there is no contact among the particles of silicon embedded in the epoxy matrix, $M < 1$ where M is the number of contacts per particle. However, the thermal diffusivity value in this region is not governed by the epoxy matrix. The inclusion of Si particles at these concentrations increases the effective thermal diffusion value by an order of magnitude (0.0021 cm^2/s for pure epoxy to 0.0178 cm^2/s at 9.35 vol% silicon). For 10 vol% $< x <$ 20 vol%, two situations are possible: (a) the system remains in dilute phase, and silicon particles are randomly well mixed in the epoxy matrix (in this case the number of contacts per particle is $M > 1$); alternatively, (b) the system displays the formation of chains or clusters. If the volume fraction of silicon particles increases, a process of random chain formation arises, and/or the interparticle conductivity also increases, giving rise to the formation of silicon chains. Theoretically, at the percolation threshold there exists an infinite interconnectivity among silicon chains and clusters, although there is no electrical conductivity. This means that the silicon particles are percolating through the epoxy matrix. When the silicon volume fraction increases from 10 to 15 vol%, it is possible that the number of contacts per particle increases, thus allowing the formation of Si chains and clusters. In this manner heat can diffuse through the matrix. This results in the observed sharp rise in the diffusivity value, seen in Fig. 5, as the Si concentration changes between 12% and 16%, close to the reported electrical percolating threshold for an rcp system [18].

Finally, for high volume fractions of silicon (region III, $x > 20$ vol%), the addition of silicon particles increases the average number of contacts

per particle to above 2 [3]. In this case, the thermal behavior is controlled by the distribution of the silicon particles. According to Every et al. [19], at high volume fractions of diamond in Zn/diamond ($x > 30$ vol%), the interconnectivity among the diamond particles appears very anisotropic as a group and theoretically the calculation of the thermal conductivity (diffusivity) for this system requires extensive information about the correlation between the relative positions of particles. This implies that different morphologies can occur as a function of the volume fraction and the effective thermal diffusivity values exhibit a nonlinear shape for high values of the volume fraction. For this reason, it is possible that the decrease in the effective thermal diffusivity values in our samples for $x > 20$ vol% is related to the morphological distribution of the silicon particles.

5.3. PTR characterization

One-dimensional and three-dimensional PTR [2,21] experiments for silicon, silicon–epoxy composites, and silicon powder were carried out between 10 Hz and 100 kHz as described above. It was found that the total PTR signal consists of two contributions: thermal-wave contribution (S_{thermal}) due to the lattice absorption contribution of silicon and epoxy, and the carrier plasma-wave contribution (S_{plasma}) due to the silicon electronic contribution, resulting in the vectorial sum [21]:

$$S_{\text{PTR}} = (S_{\text{thermal}}) + (S_{\text{plasma}}). \quad (2)$$

Fig. 6 shows the three-dimensional PTR normalized signal amplitude (a) and phase (b) for the above-mentioned oxidized p-Si wafer obtained between 10 Hz and 100 kHz. Using the three-dimensional PTR model [20], the multiparameter best fit values found for the thermoelectronic parameters were: lifetime (95 μs), electronic carrier diffusion coefficient (4.2 cm^2/s), front surface recombination velocity (300 cm/s), and thermal diffusivity (0.90 cm^2/s). The best fit curve is indicated by the solid line. The carrier diffusion length for the silicon sample was estimated to be around 199 μm. Fig. 6 shows the PTR normalized signal amplitude (a) and phase (b) for the entire set of Si–epoxy composite samples, for pure epoxy as well as p-Si wafer. In the case of pure epoxy only the thermal wave contribution is present, as expected. The normalized PTR signal amplitude exhibits a pure thermal frequency dependence of $f^{-0.5}$, with a flat phase for frequencies up to 10 kHz. This is the expected behavior for one-dimensional PTR. For frequencies higher than 10 kHz the phase, which is the more sensitive channel, increases [2,20]. This behavior could be attributed to microparticle dispersion. In the case of the crystalline p-Si sample, the main contribution due to electronic carrier diffusion and recombination is seen to dominate the PTR signal for the entire frequency range [19,20].

The PTR signal amplitude for the Si–epoxy composites approaches the pure silicon signal as the Si volume fraction is increased (see Fig. 6). In the PTR phase two kinds of behavior are present: (1) at low frequencies (<10 kHz), the signal phase tends toward the pure silicon signal phase as a function of increasing Si volume fraction, indicating that there is a remaining plasma component due to the Si particles even if the average particle size is smaller than the carrier diffusion length of pure Si and (2) at high frequencies (>10 kHz), there is an additional effect, as the phase lag is reversed as a function of Si volume fraction, with a monotonic decrease for samples of decreasing Si volume fraction (from Si–epoxy 32 to 6 vol%). In order to understand this high-frequency behavior, an additional experiment was carried out. The PTR signal of an Si powder on top of a pure Si wafer was measured. It was found that when the density of Si particles increases, the phase signal decreases at high frequencies and approaches the Si behavior. When there are no powder particles on top of the silicon wafer it is possible to see the remaining plasma component at low frequencies. The foregoing experiments are in agreement with the experimental PTR data reported for the Si–epoxy composites, and it is possible to establish that the increase of the phase signal at high-frequencies is related to the distribution of the silicon particles.

For the low-frequency (<10 kHz) PTR signal, the PTR thermal model with optical absorption was used to fit the data. The values obtained from

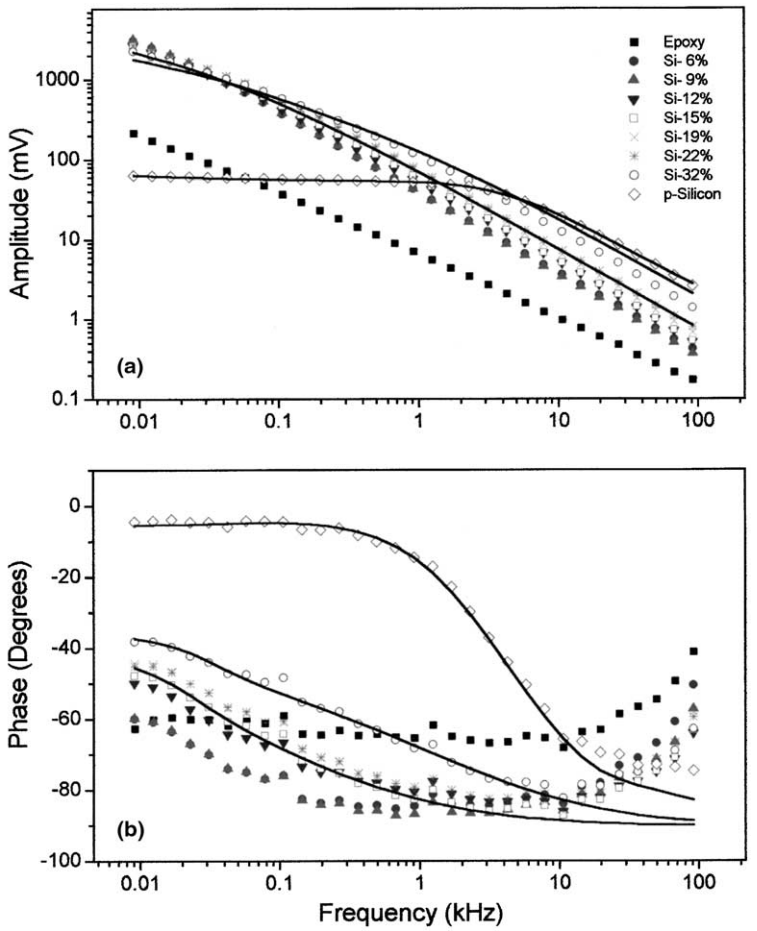

Fig. 6. PTR signal amplitude (a) and phase (b) for crystalline Si, epoxy, and Si–epoxy composite materials.

PA detection for thermal diffusivity were used in the photothermal model to obtain the optical properties of the sample assuming a constant infrared absorption coefficient for epoxy [14]. In fitting the data it is found that for frequencies lower than 100 Hz, three-dimensional effects are introduced in the sample. The full three-dimensional theoretical fitting [14] (solid lines) for 32 vol% and for 15 vol% are shown in Fig. 6. The optical absorption coefficient values for the Si–epoxy composites are shown in Table 1, where the optical absorption of silicon is also documented. It is generally found that however our experiment shows that the Si volume percentage is increased, the optical absorption rises. At 15 vol% of silicon, the optical absorption is lower than at 12 vol%. This can be attributed to the fact that at this vol%, a different morphology of silicon could have been formed, thus lowering the local optical absorption. For fitting the PTR signal in the lower concentration regime (<10 vol%), the optical scattering also has to be taken into consideration.

6. Conclusions

Using PTR measurements of Si particles, it is possible to establish their contribution to the plasma component of the signal even if their radii

are smaller than the dc carrier diffusion length $L = (D\tau)^{1/2}$. Furthermore, the electronic de-exitation process can contribute to the effective thermal diffusivity even if the major contribution arises from direct lattice Si–epoxy absorption and non-radiative conversion. The measured increase of the effective thermal diffusivity of the Si–epoxy composites could be mainly due to the presence of Si particles, and it is interesting to note that using PTR it is possible to establish the existence of an electronic contribution as well as the thermal contribution. In a complementary manner, the PA technique can monitor the total heat generated by the electronic and lattice de-excitation processes, but it is not able to distinguish between the plasma and thermal components. For this reason, it is important to use the combined PTR and PA metrologies to establish the thermal, optical, and electronic parameters in composites in the simultaneous presence of plasma and thermal components.

In conclusion, the Si–epoxy composite system (rcp) exhibits strong thermal and electronic barrier formation, presumably via the insulating SiO_2 thin films grown on the surface of Si particles, as is evident from our electrical measurements. The effective thermal diffusivity and optical absorption coefficient values of this composite exhibit an anomalous behavior around 16% Si volume fraction, which corresponds to the existence of a particle percolation threshold for three-dimensional rcp materials [18]. The combined PA and PTR results show that even though there exists an electrical barrier of very high resistivity, the composite nevertheless allows conduction of heat by means of random lattice vibrations (conduction) and heat release (by electronic de-excitation processes) that is converted into translational energy and eventually into heat at the particle surface. According to the results reported in the present work, the existence of a percolation phenomenon similar to electrical percolation can be monitored both thermally and optically in Si–epoxy composites via combined photothermal and PA detection. The problem of thermal barriers could be further studied by changing the particle size and distributions.

Acknowledgements

This work was partially supported by CONACyT (32456-E), Mexico, and Material and Manufacturing Ontario (MMO), Toronto, Ont., Canada.

References

[1] A. Mandelis (Ed.), Photoacoustic and Thermal Wave Phenomena in Semiconductors, North-Holland, New York, 1987.
[2] A. Mandelis, Solid State Electron. 42 (1998) 1.
[3] D.S. Mclachlan, M. Blaskiewicz, R.E. Newnham, J. Am. Ceram. Soc. 73 (1990) 2187.
[4] M.E. Rodríguez, J.J. Perez Bueno, O. Zelaya-Angel, J. Gonzalez, Mater. Lett. 36 (1998) 95.
[5] C.-W. Nan, R. Birringer, D.R. Clarke, H. Gleiter, J. Appl. Phys. 81 (1997) 6692.
[6] C.M. Bhandari, D.M. Rowe, Thermal Conduction in Semiconductors, Wiley, New York, 1988.
[7] M.E. Rodríguez, H. Vargas, I. Delgadillo, O. Zelaya, J.J. Alvarado, F. Sánchez, L. Baños, Phys. Stat. Sol. (a) 158 (1996) 67.
[8] H. Vargas, L.C.M. Miranda, Phys. Rep. 161 (1983) 43.
[9] M.V. Marquezini, N. Cella, A.M. Mansanares, H. Vargas, L.C.M. Miranda, Meas. Sci. Technol. 2 (1991) 396.
[10] A. Rosencwaig, Photoacoustics and Photoacoustic Spectroscopy, in: P.J. Elving, J.D. Winefordner (Eds.), Chemical Analysis, Vol. 57, Wiley, New York, 1980.
[11] A.P. Neto, H. Vargas, N.F. Leite, L.C.M. Miranda, Phys. Rev. B. 41 (1990) 9961.
[12] A. Rosencwaig, A. Gersho, J. Appl. Phys. 47 (1976) 64.
[13] S. Sheard, M. Somekh, in: A. Mandelis (Ed.), Progress in Photothermal and Photoacoustic Science and Technology, Vol. 2: Non-Destructive Evaluation (NDE), Prentice-Hall, Englewood Cliffs, NJ, 1994, Chapter 5, p. 112.
[14] A. Mandelis, L. Nicolaides, Y. Chen, I.A. Vitkin, SPIE Proc. Vol., Photonics, January 2000.
[15] A. Dargys, J. Kundrotas, Handbook on Physical Properties of Ge, Si, GaAs and InP, Vilnius, Science and Encyclopedia Publishers, 1994, p. 114.
[16] S.M. Sze, Physics of Semiconductor Devices, Wiley, New York, 1981, p. 852.
[17] L.J. Inglehart, J. Appl. Phys. 68 (1990) 2992.
[18] R. Zallen, The Physics of Amorphous Solids, Wiley, New York, 1983.
[19] A.G. Every, Y. Tzou, D.P. Hasselman, R. Raj, Acta Metall. Mater. 40 (1992) 123.
[20] A. Salnick, A. Mandelis, C. Jean, Appl. Phys. Lett. 69 (1996) 2522.
[21] M.E. Rodríguez, A. Mandelis, L. Nicolaides, J. Garcia, J. Riopel, J. Electrochem. Soc. 147 (2) (2000) 687.